The manuscript of the paper which has been published in Journal of Photochemistry and Photobiology B: Biology, Elsevier BV (Netherlands), V. 127, p. 38-51

Ultraviolet Resources over Northern Eurasia

Natalia Chubarova and Yekaterina Zhdanova

Moscow State University, Faculty of Geography, Moscow, Russia, 119991

Corresponding author: Natalia Chubarova , email: chubarova@geogr.msu.ru, tel. +7495-9392337

Abstract. We propose a new climatology of UV resources over Northern Eurasia, which includes the assessments of both detrimental (erythema) and positive (vitamin D synthesis) effects of ultraviolet radiation on human health. The UV resources are defined by using several classes and subclasses - UV deficiency, UV optimum, and UV excess - for 6 different skin types. To better quantifying the vitamin D irradiance threshold we accounted for an open body fraction *S* as a function of effective air temperature. The spatial and temporal distribution of UV resources was estimated by radiative transfer (RT) modeling (8 stream DISORT RT code) with 1x1 degree grid and monthly resolution. For this purpose special datasets of main input geophysical parameters (total ozone content, aerosol characteristics, surface UV albedo, UV cloud modification factor) have been created over the territory of Northern Eurasia. The new approaches were used to retrieve aerosol parameters and cloud modification factor in the UV spectral region. As a result, the UV resources were obtained for clear-sky and mean cloudy conditions for different skin types. We show that the distribution of UV deficiency, UV optimum and UV excess is regulated by various geophysical parameters (mainly, total ozone, cloudiness and open body fraction) and can significantly deviate from latitudinal dependence. We also show that the UV optimum conditions can be simultaneously observed for people with different skin types (for example, for 4-5 skin types at the same time in spring over Western Europe). These UV optimum conditions for different skin types occupy a much larger territory over Europe than that over Asia.

Keywords: UV irradiance, cloud modification factor, aerosol properties, RT modeling, UV resources, Northern Eurasia, skin type, vitamin D, erythema, UV optimum conditions

1. Introduction

UV radiation has a large influence on human health. Its negative effects (erythema, skin cancer, immune suppression and eye disease) and positive (vitamin D synthesis) influence on human health are well known [1]. However, skin undergoes the most significant UV impact. Therefore, in attributing UV health effects, the cutaneous negative effects (erythema, skin cancer) and cutaneous positive effects (vitamin D production) are usually considered.

There are a lot of studies devoted to the analysis of biologically active UV radiation (see the recent overviews in [1],[2],[3]), which are based on both model and experimental data. The spatial and temporal variations of erythemally-weighted or vitamin D synthesis irradiances were studied, for example, in [4],[5],[6],[7],[8],[9],[10], but in most publications the analysis was carried out separately for different types of biologically active UV radiation. The temporal and spatial distribution of erythemally-weighted irradiance over Europe was thoroughly examined in [8]. The UV climatology within 65°S-65°N was described in [10]. The UV index (*UVI*) and vitamin D climatologies in North America using ground-based UV network were presented in [4],[5]. For New Zealand the UV atlas has been developed [6]. The fast radiative transfer (RT) code for the calculation of the vitamin D synthesis duration was proposed in [7], which was further applied to assess its temporal and spatial distribution over different latitudes and seasons.

The objective of this study is to characterize the spatial and temporal UV distribution over Northern Eurasia using both erythemally-weighted and vitamin D irradiances through the classification of UV resources in the categories of UV deficiency, UV optimum and UV excess. However, for defining these categories one need to know the UV deficiency and UV excess thresholds. A well-known approach based on evaluating the different categories of UV index or Minimal Erythemal Dose (*MED*) is usually used for the estimation of the UV excess threshold [11][12]. However, there are different methods for calculating the UV deficiency threshold, which characterizes the UV level which is necessary for vitamin D synthesis [5], [7], [9], [13], [14], [15]. In some of the methods a certain level of erythemally-weighted irradiance is applied for quantifying the vitamin D synthesis threshold [13],[15]. Some of them are based on converting the vitamin D synthesis threshold from erythemally-weighted irradiance in certain conditions [5][14]. In [9] an algorithm was developed to relate vitamin D production to the erythemally-weighted irradiance using the ratio between the two quantities. Our objective was to define the most appropriate method and to apply it for estimating the UV resources for different conditions over Northern Eurasia. It should be noted that in this analysis the territory of Northern Eurasia includes the northern part of the Eurasian continent within the boundaries of 40°-80°N, 15°W-180°E. Unfortunately, the dense ground-based UV spectral network is located only in Western Europe, which makes impossible to apply these high-quality measurements in our study. An accurate radiative transfer modeling can be used instead. Recently, new accurate RT algorithms have been developed, which provide a small

uncertainty of estimations [16]. However, the main problem with the model approach, which can lead to large biases in the estimates, is the uncertainty in temporal and spatial distribution of the input atmospheric parameters. The most important input parameters for UV irradiance calculations include total ozone content, aerosol properties of the atmosphere, surface albedo and cloud attenuation in UV region of spectrum. To obtain their distribution one can use different retrievals from satellite instruments to get full coverage of the territory with a good spatial resolution. However, there are some problems with obtaining the reliable aerosol and cloud parameters using the existing methods especially in snow conditions. The climatology on aerosol optical thickness in the UV spectral region has been generated only over Europe [17]. The spatial distribution of cloud reflectivity was obtained only for snow-free conditions [18],[19]. Therefore, it was important to develop reliable aerosol and cloud attenuation datasets over Northern Eurasia, which can be used for UV radiation modeling.

2. Method and datasets

2.1 Definition of UV resources

Erythema skin damage is usually quantified using *MED* (minimum erythemal dose [11]), which is different for *j* various skin types according to:

$$MED_j = \int_0^{t_{MED\,j}} \int_{\lambda_1=280nm}^{\lambda_2=400nm} Q_\lambda F_{ery\lambda} d\lambda dt = \int_0^{t_{MED_j}} Q_{ery} dt \qquad (1)$$

where Q_λ is the spectral irradiance $Wm^{-2}nm^{-1}$,
$F_{ery\,\lambda}$ is the erythemal spectral curve [20],
Q_{ery} is the erythemally-weighted irradiance.

The *MED* values change from 200 Jm^{-2}_{eff} for the first Caucasian type of skin, which is characterized by very fair colour, up to 1000 Jm^{-2}_{eff} for the African type of skin according to the Fitzpatrick classification [21].

Correspondingly, a minimum vitamin D dose production *MvitDD* can be estimated by a similar expression using the open body fraction as an additional parameter:

$$MVitDD_j = \int_0^{t_{MVitDD_j}} \int_{\lambda_1}^{\lambda_2} \frac{Q_\lambda F_{VitD\lambda}}{S} d\lambda dt = \int_0^{t_{MVitDDj}} \frac{Q_{VitD}}{S} dt \qquad (2)$$

where Q_λ is the spectral irradiance,
$F_{VitD\,\lambda}$ is the spectral curve for vitamin D synthesis according to [13],
Q_{VitD} is the vitamin D irradiance.
S is the open body fraction.

Many studies were devoted to assessing the relationship between the erythemally-weighted and vitamin D irradiances [13], [22], [23], [24]. In order to show the difference between Q_{ery} and Q_{VitD} in sensitivity to various atmospheric parameters one can use the radiation amplification factor (*RAF*) technique [1],[25],[26]. The *RAF* analysis shows that both types of radiation have similar sensitivity to most atmospheric factors, except the sensitivity to total ozone content (RAF_X=-0.8..-1.2 for Q_{ery} and RAF_X=-1.4.. -2.3 for Q_{VitD}), and to solar elevation (RAF_{hsun}=+2 for Q_{ery} and RAF_{hsun}=+2.5 for Q_{VitD}) due to a noticeable bias of $F_{VitD\,\lambda}$ maximum to the shorter wavelengths [26].

There are several methods for evaluating the minimum vitamin D dose thresholds *MVitDD* [5], [13],[14], [23], which are based on different approaches. For the same open body fraction S=25% and for the same scales of the weighting coefficients for the vitamin D production action spectrum (see the discussion in [5]), the *MVitDD* thresholds vary from 100 Jm^{-2}_{eff} [14], 106 Jm^{-2}_{eff} [5], [23], to 120 Jm^{-2}_{eff} [13]. According to our estimates the *MVitDD* threshold for skin type 2 at midday is equal to 105 Jm^{-2}_{eff}, which is also similar to the other *MVitDD* threshold values. The estimates were based on clear sky model simulations with the 1980-1988 average ozone X=380 DU according to TOMS data for 15 March over Boston (the same reference date that was used in several other publications [5], [23]) with additional account for the average cloud modification factor obtained from the TOMS LER (Lambertian Equivalent Reflectivity) algorithm [27].

However, there were evident uncertainties in F_{vitD} curve itself mainly due to the coarse resolution of the initial data and the extrapolation from 315 nm to 330 nm [28]. Additional errors in estimating the *MVitDD* threshold can appear through converting the vitamin D radiation threshold from erythemally weighted irradiance as an inverse task, since most of the *MVitDD* estimates were obtained from *MED* or *UV* indices. Therefore, for the best estimation of vitamin D radiation effects one should know both the exact

F_{vitD} curve and the *MVitDD* threshold obtained directly from experiments with the vitamin D-weighted irradiance measurements. Currently, this information is unavailable.

At the same time, in CIE 2006 [13] there were simple recommendations of choosing the *MVitDD* threshold via *MED*: "400 IU[1] vitamin D3 would require one fifth *MED* for a one fifth body area (face, hands, forearms)". Due to the lack of current knowledge and a lot of the uncertainties mentioned above, we have followed these recommendations for estimating the *MVitDD* threshold in our approach. In addition, according to the results of recent studies and new guidelines for vitamin D [29], the level of vitamin D3 was increased from 400 IU to 600 IU, which is favorable for the different categories of people.

In this case we can rewrite the equation (2) using the relationship between the equivalent to the vitamin D synthesis of one minimal erythemal dose *MED*:

$$MvitDD_j = MED_j \frac{T_{vitD}}{E_{vitD\_MED}} \frac{}{S} \tag{3}$$

where T_{vitD}=600 IU is the threshold for vitamin D production [29], and E_{vitD_MED} =10000 IU is the equivalent to the vitamin D production of one *MED* [15]. *MED* values for different skin types were taken from [21].

Open body fraction *S* can be expressed as a function of air temperature. However, the most uncomfortable conditions, which require additional skin protection leading to *S* decrease, are observed in cold period at low temperatures accompanied with strong winds. At the same time due to small sun elevation, cold period is also characterized by critical levels of UV radiation for generating vitamin D even for a standard one-fifth open body fraction [15],[23],[24]. As a result, *S* can be calculated using effective temperature t_{eff}, which is mainly a function of air temperature with a correction on wind velocity for negative temperatures (in a first approximation) according to [30]. The t_{eff} can be parameterized by the following equation:

$$t_{eff} = t + (4.27\, V^{0.229} - 10) \tag{4}$$

where t is the air temperature in Celsius degree at 2 meters,
V is the wind velocity in ms^{-1} at 10 m.

The spatial distribution of effective temperatures for each month was obtained over the continent using the ground meteorological measurements (air temperature and wind velocity) from the dataset available at http://www.cru.uea.ac.uk/cru/data/hrg/tmc [31] with 1°x 1° grid using the equation (4).

The dependence between open body fraction *S* and effective temperature was evaluated from the combined data [30],[32] (Fig. 1). The S dependence on temperature was obtained using a simple balance model described in [31], which accounts for the thermal balance of a human body as a function of the open body fraction and the difference between skin temperature and air temperature. The final dependence can be parameterized by the following equation:

$$S(t_{eff}) = 0.141\, exp(0.041\, t_{eff}),\ R^2 = 0.98: \tag{5}$$

where R^2 is the determination coefficient.

This equation was also tested using "the rule of nines" and the comfort conditions for a human being at different effective temperatures according to the recommendations in [30]. The spatial t_{eff} distribution was applied for estimating the open body fraction *S* over Northern Eurasia, which is shown in Fig. 2a for the central months of the seasons. One can see distinct changes in *S* in winter (January) with a minimum in the North-East of Russia (less than 0.02) and a maximum in Spain (around 0.2). In summer (July) *S* distribution has a pronounced maximum (up to 0.5) over Central Asia. One can see a pronounced deviation from the latitudinal dependence over the continent in different months.

Fig.3 presents the monthly changes in the open body fraction *S* at different latitudes over specified longitudes, which reflect the influence of climate continentality on *S*. The *S* variations are characterized by much higher amplitude over the eastern part of Northern Eurasia (110 E) compared with that over Central Europe (30 E). In winter months the open body fraction in the East of the continent (40 N and 110 E) is the same as that for the far north in the West (70 N and 30 E). One can also see the specific effects of atmospheric circulation in summer at 110 E, which lead to smaller temperatures due to monsoon cloudy conditions at 50 N compared with those at 60 N and, hence, a lower open body fraction *S*.

Using the obtained *S* dataset and the *MED* values for different skin types the minimum vitamin D dose thresholds have been calculated through the equation (3). As an example, Fig. 2b,c demonstrates the obtained *MVitDD* distribution over the continent for skin types 2 and 4. One can see a dramatic 10 times difference in the *MVitDD* values varying in winter from 70 Jm^{-2}_{eff} to 760 Jm^{-2}_{eff} for skin type 2, and from 130 to 1370 Jm^{-2}_{eff} for skin type 4. In summer the difference varies from 50 to 310 Jm^{-2}_{eff} for skin type 4,

[1] IU denotes international unit: 1 IU equals to 25 ng of vitamin D [29].

and from 30 to 170 Jm^{-2}_{eff} for skin type 2, whereas for the standard specification S=0.2 [20] the *MVitDD* values are equal to 135 Jm^{-2}_{eff} and 75 Jm^{-2}_{eff} respectively for skin type 4 and 2.

Using the threshold for vitamin D synthesis (*MvitDD)* and the threshold for sunburn *(MED)* we defined different classes of UV resources using the categories of UV deficiency, UV optimum conditions and UV excess. In addition, one should determine the time restrictions on UV dose estimating since the Bunsen- Roskoe law (or the reciprocity law) between time and radiation dose rate cannot be fully applied for erythema and vitamin D synthesis effects. The boundary of its applicability lies within one hour [15], [33], so we used one hour as a limit for a potential vitamin D production or erythema (sunburn) effect at solar noon conditions (11:30-12:30 Solar Time). Hence, if at noon, at the highest solar elevations, a person does not receive the corresponding hourly *MED* or the *MvitDD* he will not receive these doses at any one hour interval during a day. Considering the vitamin D threshold (*MvitDD)* the conditions when hourly UV dose (ΣQ_{ery}) is lower than this threshold are referred to the *noon UV deficiency* category. However, in addition, the *100% UV deficiency* is defined for the conditions when it is not possible to receive vitamin D during the whole day. The application of the latter category is useful to considering the areas with the highest risk of the UV deficiency. The *UV optimum* category is determined for the conditions when it is possible to receive *MvitDD* at noon but the hourly UV dose does not exceed *MED.* For higher UV levels which exceed *MED* we propose to define several subclasses of *UV excess.* They are attributed to the thresholds depending on the WHO UV index (*UVI*) categories [11]: *moderate UV excess* category, *high UV excess* category, *very high UV excess* category, and *extremely high UV* excess category, which are respectively related to moderate, high, very high, and extremely high hourly *UVI*. However, the *UVI* thresholds are not the same for different skin types. To account for these changes the hourly *UVI* thresholds for skin type 2 (j=2) [11] are recalculated into the hourly erythemal doses for different skin types using a simple conversion: $UVI\ K_j\ 3600 / 40$, where K_j accounts for skin type difference $K_j=MED_j/MED_{j=2}$. The full classification of the UV resources is summarized in Table 1.

2.2 Description of the datasets and the simulation scheme

The UV irradiance at ground was calculated using the Tropospheric Ultraviolet and Visible (TUV) model [34] over Northern Eurasia (40°N-80°N, 15°W-180°E) for each month of a year. The TUV model has been slightly modified for a better description of aerosol and gaseous absorption. The 8 stream discrete ordinate (DISORT) RT code [35] implemented in the TUV has been applied in the calculations. This RT code was thoroughly tested against the experimental spectral data in different geographical regions [36]. The agreement between measurement and model data was found to be at the 5% level if the input atmospheric parameters were known for the model estimations [36]. Hence, for providing reliable UV irradiance estimates at ground it was necessary to obtain the veracious spatial and temporal distribution of the main atmospheric parameters (total ozone, surface albedo, aerosol and cloud characteristics). In addition, since the objective of this study was to characterize the mean UV conditions it was also necessary to keep the requirement on long-term period of observations for the retrievals of these parameters. Since the TOMS measurements on board different satellites (http://ozoneaq.gsfc.nasa.gov/) have the longest period of observations and provide the retrievals of different atmospheric parameters, these data were chosen wherever possible. However, during the polar night no data were available at high latitudes.

Fig.4 presents the spatial distribution of total ozone for different months over Northern Eurasia from the TOMS data. The seasonal changes in ozone distribution with a maximum in spring (up to 470 DU) and minimum in autumn (up to 270 DU) are associated with photochemical and dynamical processes in the atmosphere [37]. The synoptic tropospheric vortex can play an essential role in perturbating the latitudinal character of ozone distribution. For example, during the cold period (December-March) a significant increase in ozone over the Far East is explained by intensive systems of Aleutian cyclones with additional advection of rich ozone air from the North.

TOMS data were also used for retrievals of the UV surface albedo (*As*) climatology. For this purpose a Moving Time-Window (MTW) technique [38],[39] was applied to the 360 nm Nimbus-7 TOMS data. This method is based on the assumption that the reflectivity values within a certain time-window around the day of interest form a sample of the reflectivity distribution whose lower tail corresponds to the clear sky case. An estimate of the surface albedo is obtained by fitting a linear function to the lower tail of the cumulative distribution of the sample [39]. This method provides a satisfactory distinction between the cloud and snow scenes, which is very important for the development of the UV surface albedo and cloudiness climatology for relatively high surface albedo conditions during the cold period. The comparison of monthly mean MTW surface albedo over Moscow against the *As* retrievals from ground-based measurements [40][41] and from the MODIS MCD43C3 dataset (As_{MODIS}) [42][43] has revealed a satisfactory agreement within 0.02-0.1 for winter months with snow cover (Table 2). It is necessary to note that for the vegetation period As_{MODIS} due to measurements in the visible spectral region should be higher than UV surface albedo, but it should be similar in snow conditions, which is the subject of interest in this comparison. The resulting spatial UV surface albedo distribution (As_{MTW}) over Northern Eurasia is shown in Fig. 5. As_{MTW} changes in a wide range from 0.02 for green grass to 0.9 over the arctic desert areas. In winter, central parts of the continent with steppes and deserts covered by snow are also characterized by higher surface albedo of up to 0.60-0.75 while the *As* values in the forest regions (for example, over Central European Plain) do not exceed 0.3-0.4 due to the much lower reflectivity of dark trees compared with pure snow reflectivity.

For characterizing the distribution of aerosol optical thickness in UV region (λ=380nm) the composite maps have been developed for each month of the year based on the MODIS AOT550 dataset (version 5.0) over the 2000-2008 period, the data from

ground-based AERONET network (1994-2006) and the Russian actinometrical network (1980-2003). First, a spatial distribution of aerosol optical thickness in the visible region was obtained, which then was recalculated to the UV spectral range at 380 nm using the Angstrom parameter (α=-dln(AOT_λ)/dln(λ)) from the AERONET climatology over the 5 selected regions with different aerosol types. In addition, special filters were applied to the initial MODIS data to avoid large biases, which were located mainly over the areas near bright snow surfaces. All suspicious data and the gaps over the bright surfaces were substituted with the surface AOT climatology. Fig. 6 shows the final AOT380 spatial distribution over Northern Eurasia, which is characterized by significant changes from AOT_{380}=0.02 over northern areas in cold season to AOT_{380}=0.8-1 over the central regions of the continent in summer. Since no reliable data on spatial and seasonal distribution of aerosol single scattering albedo (SSA) and asymmetry factor (AF) are available, we used mean values (SSA=0.94, AF=0.75), which were obtained from the AERONET dataset with further recalculation to the UV spectral region. Similar procedures were applied for the evaluation of spatial distribution of aerosol optical thickness in the UV spectral region over Europe [17].

When evaluating cloud modification factor *CMF* (*CMF*=Q_{cloudy}/Q_{clear}) a new approach was used to obtain more accurate results for the conditions with high UV surface albedo using the standard TOMS/OMI *LER* data together with the additional information on the low layer cloud amount. The proposed method is based on the assumption that one pixel of TOMS/OMI *LER* can be presented in the form of two components: the clear and cloudy components with weighting coefficients, which are available from the independent low layer cloud amount ECMWF ERA Interim reanalysis dataset:

$$LER=(1-N)\,As+R_{cloud}\,N, \quad (6)$$

where *N* is the low level cloud amount from the ECMWF Era Interim dataset (1979-2002) expressed as a fraction. The choice of ECMWF Era Interim (1979-2002) dataset was discussed in [46];

As is the surface albedo from MTW TOMS *LER* (1979-1992) approach [39];

R_{cloud} is the low level cloud reflectivity;

LER is the total TOMS UV Reflectivity (1979-2002).

Due to the low aerosol content in winter conditions [17] one can neglect the small aerosol absorption and hence, can present *CMF* for non-absorbing conditions using the characteristics, which are available from the different retrieval algorithms, as follows:

$$CMF=1-R_{cloud}\,N \quad (7)$$

$$CMF=1-(LER-(1-N)As) \quad (8)$$

The calculated *CMFs* were tested against Moscow data CMF_{MOMSU}, which were obtained on the base of long-term measurements of erythemally-weighted irradiance (1999-2006) by UVB-1 YES pyranometers [40] at the Meteorological Observatory of Moscow State University (MOMSU). The additional comparisons were made with the cloud UV transmission estimates, obtained by the standard TOMS *LER* approach [27] (see Table 2). One can see that for winter conditions with high surface albedo the *CMFs* from the proposed method are in better agreement with the experimental data in comparison with the results obtained from the standard TOMS *LER* approach: all the *CMF* estimates (except the *CMF* obtained for January) lie within the variations of the experimental *CMFs*, which are about 0.05-0.11 at P=95%. In January due to specific weather conditions the statistics on Q_{clear}, necessary for the *CMF* evaluation, were very small (n=8), which could lead to unrealistically high experimental *CMFs*. The standard *LER* algorithm in snow conditions provides 30-50% lower *CMFs* values relative to the experimental data, since the *LER* algorithm is not sensitive to surface albedo at large cloud optical thickness [45],[46]. At the same time, in winter there is a significant increase in the surface UV level due to the effects of multiple scattering between a highly reflected surface and the cloud bottom. During warm period the *CMF* retrievals obtained by different methods are in satisfactory agreement with the difference between various *CMF* estimates lying within the uncertainty of empirical *CMF* evaluation at the Meteorological Observatory of Moscow State University, which is about 0.03-0.08 for various months without snow cover (May-September).

Using the proposed approach we estimated the monthly *CMF* distribution, which is characterized by the significant spatial and temporal variations (Fig. 7). This variability reflects significant changes in different synoptic processes over Northern Eurasia. In winter, for example, one can see a decrease in *CMFs* due to the enhanced cyclonic activity in midlatitudes over Europe (up to 0.3-0.4) and a *CMF* increase due to the influence of the Siberian anticyclone (CMF= 0.8-0.9) over the central part of the continent. In summer *CMF* growth is observed over the southern European region (higher than 0.9) due to the influence of the Azores anticyclone, which spreads its impact up to the central parts of Northern Eurasia.

All the datasets described above were used as the input parameters for RT modeling. First, on the base of the 8 stream DISORT RT code the electronic tables (LUTs) were generated, which contained the results of estimated clear sky UV irradiance over the large range of different parameters with the discretion of *dh*=1° for solar elevation within *h*=1°-90°, *dAOT380*=0.02 for aerosol optical thickness at 380 nm within *AOT380*=0.0-0.98, *dAs*=0.1 for surface albedo within 0.0-1.0, and *dX* =20 DU for total ozone content over *X*=150-490 DU. These LUTs were further applied for estimating the UV doses with the uncertainty of the final calculations including interpolating of less than 1 %. A 3 minute time interval was chosen for hourly and daily doses estimates. The results of radiative

calculations were matched to the real Sun-Earth distance. The *CMF* correction was applied later for calculating the UV irradiance in mean cloudy conditions. The total scheme applied for the simulation of the UV resources is shown in Fig. 8. The monthly UV doses were estimated over noon 11:30:12:30 Solar Time (ST) and over daytime for different types of skin according to the Fitzpatrick classification [21] for clear and mean cloudy conditions. The examples of hourly noon UV index spatial distribution for the central months of the seasons are shown in Fig. 9 for clear sky and cloudy conditions. One can see the significant effects of cloudiness, which in some months dramatically change the latitudinal character of the UV index distribution. The influence of aerosol is mainly expressed in a 5-15% UV index decrease compared with calculations in the aerosol-free atmosphere. We should also mention that the areas with the absence of input data in the North in the cold period were thoroughly tested using different combinations of atmospheric parameters. It was shown that over these areas in all cases the conditions with 100% UV deficiency were obtained even for the hypothetically most favourable atmospheric parameters of a small ozone amount, a high surface albedo and a small aerosol optical thickness.

For the altitude correction, which was not accounted in the basic calculation scheme, we propose to use a simple model altitude correction factor (*ACF*). The *ACF* has been obtained within the range of ozone content 250-450 DU for solar elevations higher than 30 degrees separately for two surface albedo: A_s=0.02 and A_s=0.7. The latter value relates to the maximum estimates of spatial snow surface albedo in the mountainous area, which are about 0.5-0.7 [47],[48]. The results are shown in Table 3. In addition, the account for the aerosol optical thickness decrease with the altitude according to [8] has been made. This account provides higher *ACF* estimates of about 5-8% per kilometre for clear sky conditions (see Table 3). It is interesting that the *ACF* for the same snow albedo at different heights is significantly smaller than that for low surface albedo due to the more effective role of multiple scattering, which increases the diffuse component at zero altitude level and, to some extent, compensates for the increase of direct flux due to smaller total optical thickness at higher altitudes. The experimental data on altitude UV enhancement for Europe conditions vary within a wide range from 7% to 16% per kilometre [2]. Our simulated values taken with the account for both Rayleigh and aerosol optical thickness decrease lie within this range. An additional increase in the experimental *ACF* values can be observed due to simultaneous changes in surface albedo with altitude, by 3D effects enhancing multiple scattering, and by a possible decrease in cloud optical thickness with height. However, in a first approximation one can use the *ACF*=5-8% to apply for the UV altitude correction in the mountainous regions and, hence, update the UV resources over these particular areas. The altitude correction was not included directly in the model computations scheme because the one degree resolution used in our calculations is not an adequate spatial resolution for the mountainous regions. This could lead to an unrealistic UV level at a smoothed virtual altitude over the 1 x 1 degree grid. At the same time most of the territory of Northern Eurasia lies on the plains. Hence, we propose to account for the UV altitude dependence, when necessary, using this additional extrinsic correction for a specified altitude.

3. Results

The proposed method provides a tool for obtaining temporal and spatial distribution of UV resources over Northern Eurasia for different types of skin. We mainly focus on the detailed analysis only for skin types 2 and 4 separately for cloudless and mean cloudy conditions, which take into account for the average cloud modification factor distribution shown in Fig.7. Special attention is paid to the distribution of UV optimum area for all skin types in mean cloudy conditions.

3.1. **Main features in distribution of UV resources in clear sky conditions**

Fig. 10 presents the UV resources spatial distribution for skin type 2 and skin type 4 in cloudless conditions for the central months of a year over Northern Eurasia. One can see significant seasonal changes from almost full UV deficiency in January to the most UV excess conditions in July for both skin types due to dramatic changes in solar elevation, geographical distribution of aerosol, ozone and surface albedo as well as due to variations in the open body fraction. On the whole, seasonal variability of UV resources are larger for skin type 2 than that for skin type 4.

In January for skin type 2 the most unfavorable 100% UV deficiency conditions are shifted from 58° N in the West to 48°N in the East due to changes in the open body fraction *S* and in total ozone content (see Fig. 2 and Fig. 4). On the whole, the UV deficiency conditions occupy around 97% of the territory of Northern Eurasia for skin type 2 and over 99% - for skin type 4 (hereinafter, for simplicity the percentage of the territory means the percentage of 1x1°grid number). In Western Europe in clear skies the UV optimum conditions can be observed only southward of 48°N. This distribution is mainly explained by the lower total ozone content and, to some extent, by the lower aerosol optical thickness over this area. For skin type 4 there is a distinct bias of the UV optimum area towards the South mainly due to the higher threshold on vitamin D production (compare Fig. 2b and Fig. 2c). As a result, people with this type of skin can obtain optimum UV radiation only southward of 43°N in Spain and nearby territories that occupies less than 0.4% of the territory. At the same time, around 80% of Northern Eurasia is characterized by the most adverse 100% UV deficiency conditions.

In April the UV deficiency conditions are observed over much smaller areas: 24% for skin type 2 and 45% for skin type 4. For skin type 2 the territory with the noon UV deficiency is shifted northward of 70°N in the West and northward of 62°N in the East. The

observed bias from the latitudinal distribution is explained by the total ozone maximum over the Far East region as well as the *S* increase to the West. Note, that no territories, which are characterized by the 100% UV deficiency, are observed for skin type 2. However, for skin type 4 the 100% UV deficiency is observed in less than 0.1% of cases over the far northern areas in the central part of the continent due to low temperatures, which affects the open body fraction in conditions of relatively small UV doses. For skin type 2 the UV optimum conditions, when it is possible to receive necessary UV dose for vitamin D production but no sunburn, are observed over 59°-70°N occupying larger areas in the West than in the East. These changes are explained by the increase in surface albedo that expands the area with the UV excess conditions, and by lowering the open body fraction, that increases the MvitDD threshold and, hence, leads to the growth of the UV deficiency area. For skin type 4 the UV optimum conditions are observed on a much larger territory from 42°N to 65°N with a bias towards the South in the Far East due to the changes in total ozone and the open body fraction *S* (see Fig. 2 and Fig. 4). However, for skin type 2 in April one can already see the moderate and high UV excess conditions in more than 50% of cases.

In July there are no conditions with UV deficiency for skin type 2 and less than 0.2% of cases are characterized by the noon UV deficiency conditions for skin type 4. At the same time, only 1% of cases are characterized by the UV optimum conditions for skin type 2 which are observed in the Far North, however, for skin type 4 the UV optimum conditions occupy much larger area northward of 60°N with almost the same size of about 40% as in April. Due to small changes in ozone the spatial distribution of UV resources has a latitudinal character with a total bias towards lower latitudes due to the AOT increase. For skin type 2 the conditions of very high UV excess are observed southward of 45°N-48°N, however, for skin type 4 due to much larger *MED* only the moderate UV excess conditions over the territory southward of 60°N can be seen.

In October due to the decrease in solar elevation the UV deficiency conditions are prevailed for both skin types (52% and 67% correspondingly). For skin type 2 the large area with the 100% UV deficiency conditions are observed northward of 70°N in the central parts of the continent with the bias towards 65°N in the East due to the increase in total ozone and in open body fraction. The area with the UV optimum conditions (32% of the territory) lies southward of 60°N in the West and southward of 51°N in the East due to the same reasons. Around 16% of the territory southward of 47°N is characterized by the moderate UV excess conditions. Some local features of higher UV level in the central part of the continent are explained by the surface albedo increase and smaller aerosol optical thickness. For skin type 4 no conditions with UV excess are observed and all the boundaries of UV resources are shifted to 5-10° towards the South compared with those for skin type 2.

3.2. **Main features in distribution of UV resources in mean cloudy conditions.**

Since clouds significantly attenuate UV irradiance the borders of UV resources should have a bias towards lower latitudes compared with their distribution in clear sky conditions (Fig. 11). However, cloud modification factor, which is mainly a function of cloud optical thickness and cloud amount, varies significantly in time and space (see Fig. 7) and, as a result, provides different pictures of UV resources distribution.

In January the conditions of UV deficiency are observed in 99-100% of cases both for skin type 2 and skin type 4. At the same time, the area occupied by the most adverse 100% UV deficiency conditions is almost 10% larger than that observed in clear sky conditions. However, in spite of cloud attenuation the UV optimum conditions for skin type 2 are still observed over the northern part of Spain and Italy southward of 43°N, covering only 1% of the territory of Northern Eurasia. This is explained by relatively high cloud modification factor (higher 0.7) over this area. At the same time no UV optimum is observed for skin type 4 in January at the territory of Northern Eurasia.

In April one can see much larger area with the UV deficiency of about 37% for skin type 2 and 54% for skin type 4. The 100% deficiency is shifted northward of 71°N and 68°N respectively. The UV optimum conditions for both skin types are also observed over larger area (28% and 43% respectively), however, their distribution, especially for skin type 2, has sometimes a spotty character due to significant spatial variations in cloud modification factor. The approximate boundaries of this zone for skin type 2 lie between 47°-49°N and 62°-65°N with 5-10° shift towards equator relative to their location in clear sky conditions. For skin type 4 the UV optimum conditions are observed within 40°-61°N, while only 3% of the territory is characterized by the moderate UV excess conditions. The *CMF* increase over the central regions of the continent leads to larger UV level and to a noticeable shift of the UV optimum towards the North especially for skin type 2. For this skin type the UV excess is observed in 35% of cases that is much less than in clear sky conditions.

In July in mean cloudy conditions over Northern Eurasia the UV excess is prevailed for skin type 2 (83% of cases) and the UV optimum – for skin type 4 (69% of cases). Note, that there are only 1-2% of cases with the UV deficiency conditions for both skin types. For skin type 2 the UV optimum conditions are observed northward of 63°N with a boundary biased towards lower latitudes over Scandinavia and Far East due to the more active cyclonic activity and the decrease in *CMF*. For skin type 4 the UV optimum zone is observed over most of the continent except small northern areas higher 73°N with a shift towards the North over the central part of the continent due to the increase in *CMF*.

In October the UV deficiency conditions are observed over the most territory of Northern Eurasia for both skin types (63% and 77%, respectively, for skin type 2 and 4). Large areas of the continent are characterized by 100% UV deficiency conditions (29% and

42%). For skin type 2 these areas can be seen northward of 61°-66°N and for skin type 4 - northward of 56°-62°N with a distinct shift to the North in the West due to the increase in open body fraction and smaller ozone content. The UV optimum conditions cover almost the same size of the territory (32%) like that in clear sky conditions but this area is shifted towards the South from approximately 43°N to 52°-57°N. For skin type 4 the UV optimum area is observed southward of 46°-51°N. For skin type 2 only 6% of cases with the UV excess conditions are observed southward of 44°N and for skin type 4 there are no such conditions while in clear sky situations they are observed in 16% of cases.

3.3. **UV optimum for different skin types in mean cloudy conditions.**

A particular attention was paid to the joint analysis of the UV optimum spatial distribution for different skin types in mean cloudy conditions. The most favourable situation is considered, when the UV optimum is observed for several skin types over the same area at the same time. Fig. 12 shows the distribution of the UV optimum conditions for different skin types. One can see that the UV optimum can be observed for one skin type or for up to 5 skin types simultaneously. The conditions, when the UV optimum for 5 skin types is observed at once, take place very rarely: just in 2% of cases in October for people with skin types from 1 to 5. However, the situations with the simultaneous UV optimum for 3 or for 4 skin types can be observed quite often. For example, in July the UV optimum conditions for skin types 2, 3, 4, and 5 can be observed simultaneously in 12% of cases, whereas for skin types 4, 5, 6 - in 40% of cases.

In winter (January), the UV deficiency conditions are prevailed for almost all skin types over the whole continent. Only in Spain one can see the simultaneous UV optimum for people with skin types 1, 2, and 3. This zone has a noticeable bias towards the South in the East due to total ozone increase and decrease in the open body fraction *S*.

In April 70% of Northern Eurasia is characterized by the UV optimum conditions, however, there is a pronounced difference in distribution of the UV optimum for different skin types. The UV optimum for 4 skin types is simultaneously observed in 9% of cases, mainly, over Europe. At the same time, around 40% of cases are referred to the simultaneous UV optimum conditions for people with 3 or 4 different skin types. One can see that this UV optimum area also occupies larger territory in the West than in the East of the continent. The spatial changes in the UV optimum conditions for different skin types correlate well with the distribution of skin types themselves with fair skin in the North and dark skin in the South. There is also a tendency of the UV optimum shift towards the South in the Far East due to the total ozone increase. Also the inverse shift of the UV optimum conditions for skin types 5 and 6 over the central part of the continent is explained by less cloud attenuation and the presence of snow with high surface albedo in the northern part of this area.

In July more than 40% of the territory is characterized by the simultaneously observed UV optimum for skin type 4, 5, and 6, while about 20% of the territory is referred to the UV optimum for skin type 5 and 6. At the same time, the UV optimum conditions for skin type 1 alone or in combination with other skin types are observed only over 3% of the territory shifted to the North of 70°N. One can also see approximately latitudinal character in the UV optimum distribution for different skin types, except over the southern Far East, which is characterized by stronger cloud attenuation due to summer monsoon.

In October the UV optimum conditions are observed over 45% of the territory of Northern Eurasia with a significant southern shift to the East of the continent due to the decrease in open body fraction and the increase in total ozone. The simultaneously observed UV optimum conditions for skin types 1-4 and 1-5 can be seen over Central Europe from 45° to 52°N and, again, the size of this comfortable zone for many skin types noticeably decreases towards the East. The UV optimum conditions for dark skin (6 skin type) are observed only southward of 42°N.

4. Discussion and conclusions

We propose a new approach for the classification of UV resources, which accounts for both detrimental (erythema) and positive (vitamin D synthesis) effects of ultraviolet radiation and can be useful in different applications. This approach was used for evaluating favourable and adverse UV conditions in different months over the territory of Northern Eurasia. In order to better quantify the vitamin D synthesis threshold (*MvitDD*) a parameterization of the open body fraction *S* as a function of surface effective temperature has been obtained. Using both *MvitDD* and *MED* thresholds and the different standard UV index categories [11] the spatial distribution of UV resources was assessed over Northern Eurasia with the 1 x 1°grid for clear and mean cloudy conditions using RT modeling on the base of the developed datasets of main atmospheric input parameters.

Testing shows an agreement of the *MvitDD* calculations with the results obtained, for example, in Boston [49], where the vitamin D deficiency conditions were observed in February, but vitamin D synthesis was possible in March. However, as we showed, the 42°N latitude boundary for vitamin D synthesis mentioned there, can significantly vary due to the spatial changes of different atmospheric factors and open body fraction and, as a result, can differ dramatically from the latitudinal distribution. We can also note

that the inconsistency in geographical and seasonal distribution of vitamin D deficiency mentioned, for example, in [9] can be attributed, to some extent, to non accounting for the temporal and spatial variations in the open body fraction.

There are significant seasonal changes of UV resources over the continent - from almost full 100% UV deficiency in January to the domination of the UV excess conditions in July for different skin types due to changes in solar elevation and variations in spatial distribution of aerosol, ozone, surface albedo, cloudiness as well as open body fraction. Seasonal variations were shown to be the largest for fair skin (skin type 1 and 2) compared with dark skin (skin type 4, 5, 6).

There is a significant bias of about 5-10° towards the South for different types of UV resources in cloudy conditions compared with those in clear sky. There is also a noticeable shift of all UV resources zones almost in all seasons towards the South in the East of the continent due to the difference in open body fraction, total ozone and cloudiness.

The UV optimum in mean cloudy conditions can be simultaneously observed for people with 4-5 different skin types. For example, more than 25% of cases are characterized by the joint UV optimum for 4 or 5 skin types in July, and about 17% of cases - in October. More often these conditions are simultaneously observed for 3 or more skin types (39% in April, 69% in July, and 31% in October). These favourable UV optimum conditions for people with different skin types occupy larger territories in the West than in the East of the continent.

The results obtained for different skin types show that in winter (January) in mean cloudy situations favourable UV optimum conditions are observed only over the small area (2% of cases) in the South-West of Europe for skin types 1, 2, 3. In spring (April) almost 70% of Northern Eurasia is characterized by the UV optimum conditions for different skin types. In summer (July) the UV optimum conditions are observed in 97% of cases with their prevailing for skin types 4, 5, 6. However, there are only few spots favourable for people with skin types 1 and 2 in the Far North. In autumn (October) the UV optimum conditions are observed only in 41% of cases with a significant southern shift in the East of the continent due to the decrease in open body fraction and the increase in total ozone.

We understand that the distribution of UV resources is much more complex than it was shown in our study. For example, it is necessary to take into account for different orientation of human body, human behavioral habits, the influence of the opacity of trees, buildings on UV level, etc. In addition, in this approach for simplicity we account only for the European cultural tradition and evaluate the open body fraction via its correlation with the ambient temperature, however, in other cultures (in Islam, for example) other dependences will be observed. Nevertheless, the developed approach can be used in a first approximation for evaluating the distribution of the natural UV resources, and might be useful in different applications.

Acknowledgments

We would like to thank anonymous reviewers for helpful comments. The work was partially supported by the by RFBR grant № 12-05-00877.

References

[1] J. F. Bornman, N. Paul, X.Tang. UNEP, Environmental Effects of Ozone Depletion and its Interactions with Climate Change: 2010 Assessment. United Nations Environment Programme, ISBN 92-807-2312-X. (2011).

[2] A.F. Bais, D.Lubin, A.Arola, G.Bernhard, M.Blumthaler, N.Chubarova, C.Erlick, H.P.Gies, N.Krotkov, B.Mayer, R.L.McKenzie, R.Piacentini, G. Seckmeyer, J.R.Slusser. Scientific Assessment of Ozone Depletion: 2006, Chapter 7: Surface Ultraviolet Radiation: Past, Present and Future, *World Meteorological Organization Global Ozone Research and Monitoring Project, Report,* **50.** (2007).

[3] S. Bekki, G. E. Bodeker, A.F. Bais, N. Butchart, V. P. Braesicke, A.J. Charlton-Perez, N.E. Chubarova, I. Cionni, S.B. Diaz L. N.P. Gillett S. Pawson, M.A. Giorgetta, Eyring,D.W. Fahey,D.E. Kinnison,U. Langematz, B. Mayer,R.W. Portmann, E. Rozanov Scientific Assessment of ozone Depletion: 2010, Chapter 3: Future Ozone and Its Impact on Surface UV. *World Meteorological Organization Global Ozone Research and Monitoring Project—Report,* **52** (2011).

[4] V. E. Fioletov, M.G. Kimlin, N. Krotkov, L.J.B. McArthur, J.B. Kerr, D.I. Wardle, J.R. Herman, R. Meltzer, T.W. Mathews, J. Kaurola, UV index climatology over the United States and Canada from ground-based and satellite estimates, *J. Geophys. Res*., **109,** (2004) D22308, (Doi:10.1029/2004JD004820).

[5] V.E. Fioletov, L.J.B. McArthur, T.W. Mathews, L. Marrett. Estimated ultraviolet exposure levels for a sufficient vitamin D status in North America. *J. Photochem. Photobiol. B* **100,** (2010) 57–66.

[6] G. Bodeker, J. Burrowes, R. Scott-Weekly, S. E. Nichol, and R. L. McKenzie. A UV atlas for New Zealand, in UV Radiation and its Effects, R. Soc. of N. Z., Wellington (2002).

[7] O. Engelsen, M. Brustad, L. Aksnes and E. Lund. UV Radiation, Vitamin D and Human Health: An Unfolding Controversy Daily Duration of Vitamin D Synthesis in Human Skin with Relation to Latitude, Total Ozone, Altitude, Ground Cover, Aerosols and Cloud Thickness. *J. Photochem. Photobiol. B* **81,** (2005) 1287–1290.

[8] Long term changes and climatology of UV radiation over Europe. Edited by Z. Litynska, P. Koepke, H. De Backer, J. Groebner, A. Schmalwieser, L. Vuilleumier. Final scientific report COST Action 726: UV climatology for Europe, available at: http://www.meteoschweiz.admin.ch/web/en/research/completed_projects/cost_726.Par.0011.DownloadFile.tmp/finalreport.pdf, (2010).

[9] R. L. McKenzie, J. B. Liley and L. O. Bjorn. UV radiation: balancing risks and benefits, *J. Photochem. Photobiol. B* **85,** (2009) 88–98.

[10] J. Lee-Taylor, S. Madronich, C. Fischer, and B. Mayer. A climatology of UV radiation, 1979-2000, 65S-65N, Chapter 1 in UV Radiation in Global Climate Change: Measurements, Modeling and Effects on Ecosystems, edited by W. Gao, D.L. Schmoldt, and J. Slusser, *Springer-Verlag and Tsinghua University Press*, ISBN: 978-3-642-03312-4, (2009) 1-20.

[11] World Health Organization (WHO), Global Solar UV Index A Practical Guide. WHO/SDE/OEH/02.2 (2002).

[12] K. Vanicek, Frei T., Z. Litynska, A. Schmalwieser. UV-Index for the Public, COST-713 Action, Brussels (2000) 27p.

[13] Commission Internationale de l'Eclairage (CIE), *CIE 174*, 2006.

[14] J.W. Krzyscin, J. Jarosławski, P.S. Sobolewski. A mathematical model for seasonal variability of vitamin D due to solar radiation. *J. Photochem. Photobiol.* B **105**, (2011) 106–112.

[15] M.F. Holick, Jenkins M. The UV advantage: new medical breakthroughs reveal powerful health benefits from sun exposure and tanning. I book, New York. (2003)

[16] K.N. Liou. An Introduction to Atmospheric Radiation. *International Geophysics Series.* Academic press **84** (2010).

[17] N. Chubarova. Seasonal distribution of aerosol properties over Europe and their impact on UV irradiance, *Atmos. Meas. Tech.*, **2**, (2009) 593–608.

[18] J.R. Herman, Global increase in UV irradiance during the past 30 years (1979–2008) estimated from satellite data, *J. Geophys. Res.*, **115**, (2010) D04203, (doi: 10.1029/2009JD012219).

[19] J.R. Herman, G. Labow, N.C. Hsu, and D. Larko Changes in cloud cover derived from reflectivity time series using SeaWiFS, N7-TOMS, EP-TOMS, SBUV-2, and OMI radiance data, *J. Geophys. Res.*, **114,** (2009) D01201, (doi: 10.1029/2007JD009508).

[20] Commission Internationale de l'Eclairage (CIE), CIE Research Note, *CIE Technical Collection. 1993/3*.

[21] T.B. Fitzpatrick, The validity and practicality of sun-reactive skin types I through VI, *Arch. Dermatol.* **124** (1988) 869–871.

[22] V.E. Fioletov, L.J.B. McArthur, T.W. Mathews, L. Marrett, On the relationship between erythemal and vitamin D action spectrum weighted ultraviolet radiation. *Journal of Photochemistry and Photobiology* B **95** (2009) 9–16.

[23] A.R. Webb, O. Engelsen. Ultraviolet exposure scenarios: risks of erythema from recommendations on cutaneous vitamin D synthesis, *Adv. Exp. Med. Biol*. **624** (2008) 72–85.

[24] M.G. Kimlin, W.J. Olds, M.R. Moore, Location and vitamin D synthesis: is the hypothesis valid by geophysical data? *J Photochem. Photobiol.* B **86** (2007) 234–239.

[25] C.R. Booth and S.Madronich, Radiation amplification factors: improved formulations accounts for large increases in ultraviolet radiation associated with antarctic ozone depletion. *Ultraviolet radiation in Antarctica: measurements and biological effects*. Washington, DC, (1994), 39-42.

[26] Ye. Yu. Zhdanova and N. Ye. Chubarova, The estimating of the effects of different atmospheric parameters on biologically active UV irradiance according to the data of modeling and measurements. *Atmospheric and Oceanic Optics [In Russian],* **24** (2011), 775-781.

[27] T.F. Eck, P.K. Bhartia, J.B. Kerr. Satellite Estimation of spectral UVB irradiance using TOMS derived ozone and reflectivity. *Geophys. Res. Lett.,* **22** (1995) 611-614.

[28] M. Norval, L.O. Bjorn, F.R. de Gruijl, Is the action spectrum for the UV-induced production of previtamin D3 in human skin correct, *Photochem. Photobiol. Sci.* **9** (2010) 11–17.

[29] Dietary Reference Intakes for Calcium and Vitamin D. Institute of Medicine, Food and Nutrition Board. Washington, DC: *National Academy Press,* 2010.

[30] A. Isaev. *Ecological climatology*, Moscow State University Publishing House, (2001).

[31] M. New, D. Lister, M. Hulme, I. Makin. A high-resolution data set of surface climate over global land areas, *Climate Research*, **21**, (2000) 1-2.

[32] Ye.I. Timofeeva, G.V. Fedorovich. Environmental monitoring of microclimate parameters. *NTM-Defense Publishing House,* Moscow, (2005).

[33] Ultraviolet radiation in *Health criteria of the environmental conditions 14*, WHO, Geneva, (1984) 114 p.

[34] S. Madronich, and S. Flocke. *Handbook of Environmental Chemistry*, edited by: Boule, P., Springer-Verlag, Heidelberg, (1998) 1–26.

[35] K. Stamnes, S.-C. Tsay, W. Wiscombe, I.Laszlo, DISORT, a General-Purpose Fortran Program for Discrete-Ordinate-Method Radiative Transfer in Scattering and Emitting Layered Media: Documentation of Methodology DISORT Report, v.1.1, (2000),112 p.

[36] J. Badosa, R. L. McKenzie, M. Kotkamp, J. Calb´o, J. A. Gonz´alez, P. V. Johnston, M. O'Neill, and D. J. Anderson. Towards closure between measured and modelled UV under clear skies at four diverse sites. Atmos. Chem. Phys., 7, (2007), 2817–2837.

[37] Scientific Assessment of Ozone Depletion: 2006. *World Meteorological Organization Global Ozone Research and Monitoring Project—Report.* **50** (2007).

[38] A. Tanskanen, A. Arola, J. Kujanpää. Use of the moving time-window technique to determine surface albedo from the TOMS reflectivity data, *In: Proc. SPIE* **4896** (2003) 239-250.

[39] A. Tanskanen, Lambertian Surface Albedo Climatology at 360 nm from TOMS Data Using Moving Time-Window Technique. In: *Proceedings of the XX Quadrennial Ozone Symposium, 1-8 June 2004, Kos, Greece*. (2004).

[40] N.E. Chubarova, UV variability in Moscow according to long-term UV measurements and reconstruction model. *Atmos. Chem. Phys.*, 8, (2008), 3025-3031.

[41] N. Chubarova, A. Yurova, N. Krotkov, J. Herman, PK. Bhartia. Comparisons between ground measurements of broadband UV irradiance (300 – 380 nm) and TOMS UV estimates at Moscow for 1979-2000. *Optical Engineering* **41** No 12 (2002) 3070-3081.

[42] C. B. Schaaf, J. Liu, F. Gao and A. H. Strahler. MODIS Albedo and Reflectance Anisotropy Products from Aqua and Terra, *In Land Remote Sensing and Global Environmental Change: NASA's Earch Observing System and the Science of ASTER and MODIS, Remote Sensing and Digital Image Processing Series*, Vol.11, B. Ramachandran, C. Justice, M. Abrams, Eds, Springer-Cerlag (2011) 873 pp.

[43] M. O. Román, C. B. Schaaf, P. Lewis, F. Gao, G. P. Anderson, J. L. Privette, A. H. Strahler, C. E. Woodcock, M. Barnsley, Assessing the coupling between surface albedo derived from MODIS and the fraction of diffuse skylight over spatially-characterized landscapes, *Remote Sensing of Environment*, **114** (2010) 738-760.

[44] N. Chubarova, A. Smirnov, and B.N. Holben. Aerosol properties in Moscow according to 10 years of AERONET measurements at the meteorological observatory of Moscow State University. *Geography, environment, sustainability*, 4(1) (2011) 19–32.

[45] N. A. Krotkov, J. R. Herman, P. K. Bhartia, V. Fioletov,and Z. Ahmad Satellite estimation of spectral surface UV irradiance 2. Effects of homogeneous clouds and snow. *J. Geophys. Res.,* **106,** No. D11, (2001), 11,743–11,759.

[46] Ye. Zhdanova, N. Chubarova, and Ye.I. Nezval. The method of cloud transmission estimating in UV spectral range using data of different satellite measurements and reanalysis, *AIP Conf. Proc.* **1531** (2013), c. 911-914, (doi: 10.1063/1.4804919).

[47] S. Simic, M. Fitzka, A. Schmalwieser, P. Weihs, J. Hadzimustafic. Factors affecting UV irradiance at selected wavelengths at Hoher Sonnblick, *Atmospheric Research*, **101**, Issue 4, (2011), 869–878.

[48] I. Smolskaia , Masserot D, Lenoble J, Brogniez C, de la Casinière A. Retrieval of the ultraviolet effective snow albedo during 1998 winter campaign in the French Alps. *Appl Opt. (*2003); 42(9):1583-7.

[49] A.R. Webb, L. Kline, M.F. Holick. Influence of season and latitude on the cutaneous synthesis of vitamin D3: exposure to winter sunlight in Boston and Edmonton will not promote vitamin D3 synthesis in human skin, *J. Clin. Endocrinol. Metab.* **67** (1988) 373–378.

List of the Tables:

Table 1. The classification of UV resources.

The name of a category	Conditions:
100% UV deficiency for *j* type of skin;	$MvitDD_j > \Sigma Q_{ery}$ *(daytime)*
Noon UV deficiency for *j* type of skin;	$MvitDD_j > \Sigma Q_{ery}$ *(noon hour)*
UV optimum for *j* type of skin;	$MvitDD_j < \Sigma Q_{ery} < MED_j$ *(noon hour)*
Moderate UV excess for *j* type of skin.	$MED_j < \Sigma Q_{ery} \le UVI_{moderate\_type\ j=2} K_j\ 3600 / 40$, *(noon hour)* ($UVI_{moderate\_type\ j=2} = 5.5$)
High UV excess for *j* type of skin.	$UVI_{moderate\_type\ j=2} K_j\ 3600 / 40 < \Sigma Q_{ery} \le UVI_{high\ j=2} K_j\ 3600 / 40$, *(noon hour)* ($UVI_{high\ j=2} = 7.5$)
Very high UV excess for *j* type of skin.	$UVI_{high\ j=2} K_j\ 3600 / 40 < \Sigma Q_{ery} \le UVI_{very\ high\ j=2} K_j\ 3600 / 40$ *(noon hour)* ($UVI_{very\ high\ j=2} = 10.5$)
Extremely high UV excess for *j* type of skin.	$UVI_{very\ high\ j=2} K_j\ 3600 / 40 < \Sigma Q_{ery}$

Comment:

$K_j = MED_j / MED_{j=2}$. ($K_j = 0.8, 1, 1.2, 1.8, 2.4, 4$ for 6 skin types from $j=1$ to $j=6$ respectively).

Table 2. Monthly values of surface albedo (*As*) and cloud modification factor (*CMF*) obtained according to different methods over Moscow.

Month	Surface Albedo(*As*)			*CMF* according to the equation (8)	*CMF* according to the standard *LER* approach [2]	CMF_{MOMSU} experimental values, Meteorological Observatory, Moscow State University (MOMSU) (1999-2006)
	As_{MTW} (1979-1992)	As_{MODIS} (2001-2006)	As_{MOMSU} (2001-2006)	CMF_As_{MTW} (CMF_As_{MODIS}, CMF_As_{MOMSU})	CMF_As_{MTW}	CMF_{MOMSU} ± confidence intervals at P=95%
1	0.34	0.36	0.40	0.53 (0.53, 0.55)	0.38	0.75±0.10
2	0.36	0.34	0.39	0.60 (0.59, 0.62)	0.41	0.66±0.05
3	0.27	0.21	0.36	0.72 (0.69, 0.79)	0.58	0.73±0.06
4	0.08	0.07	0.10	0.74 (0.73, 0.75)	0.70	0.70±0.05
5	0.05	0.06	0.02	0.75 (0.77, 0.73)	0.73	0.75±0.07
6	0.04	0.06	0.02	0.71 (0.73, 0.69)	0.69	0.70±0.08
7	0.05	0.06	0.02	0.77 (0.78, 0.74)	0.75	0.74±0.03
8	0.05	0.06	0.02	0.77 (0.78, 0.74)	0.75	0.70±0.06
9	0.05	0.06	0.02	0.71 (0.72, 0.69)	0.69	0.71±0.04
10	0.07	0.06	0.05	0.59 (0.59, 0.58)	0.56	0.62±0.07
11	0.14	0.30	0.20	0.54 (0.61, 0.57)	0.47	0.51±0.07
12	0.27	0.42	0.35	0.55 (0.61, 0.58)	0.43	0.61±0.11

Comments:

As_{MTW} - MTW surface albedo climatology based on *TOMS LER* retrievals [39].

As_{MOMSU} – the *As* retrievals according to the method described in [41] with additional account for change in snow coverage [40].

As_{MODIS} – surface albedo over 0.3-0.7 μm obtained from MCD43C35 black-sky and white-sky albedo via NASA GES DISC Giovanni online data system with an additional correction on blue sky using the dependencies on solar elevation and AOT [42][43]. AOT climatology was taken from the AERONET dataset of the Meteorological Observatory of Moscow State University [44].

*CMF*s were estimated using different surface albedo values (shown in brackets).

CMF_{MOMSU} is evaluated as a ratio between monthly sums of erythemally-weighted irradiance and sums of Q_{ery} in clear sky conditions. Clear sky values were obtained from Q_{ery} empirical dependence on solar elevation for each month with additional correction on total ozone using radiation amplification factor $RAF_{X.}$.

Table 3. Altitude correction factor *ACF* for UV erythemally-weighted irradiance calculated for different conditions. R^2 – determination coefficient of the regression equations.

	Surface albedo As=0.02, in % per km	Surface albedo As=0.7, in % per km
TUV model calculation with the same atmospheric parameters at the different altitudes, AOT_{380}=0.25	6 % (R^2=0.98)	3.5% (R^2=0.98)
TUV model calculation with accounting for the aerosol decrease with altitude according to [8].	8% (R^2=0.95)	5 % (R^2=0.88)

Figures:

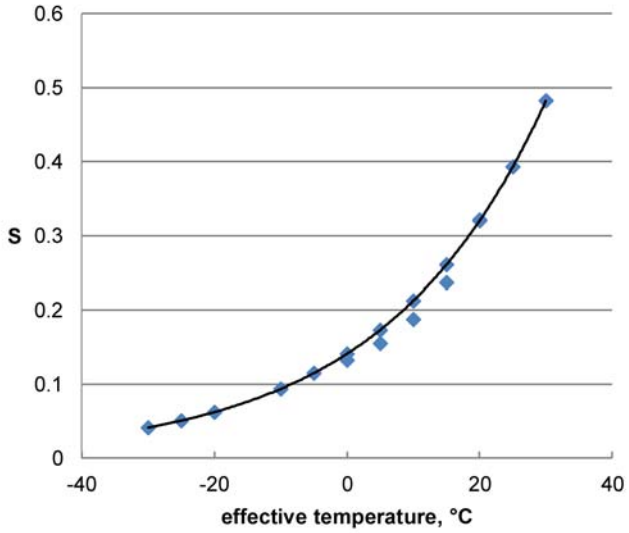

Fig. 1. The dependence of the open body fraction *S* as a function of effective temperature.

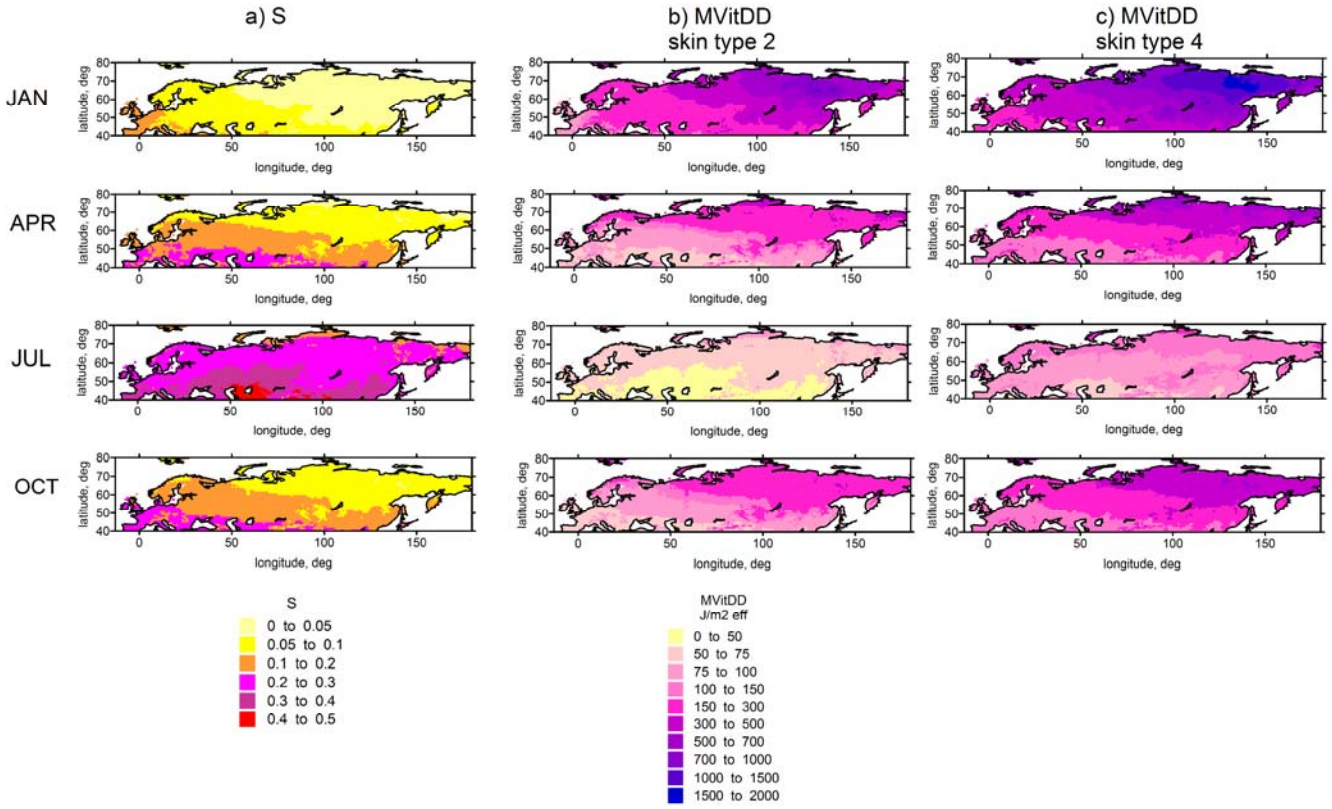

Fig. 2. Spatial distribution of the open body fraction *S* over Northern Eurasia (a), *MVitDD* distribution for skin type 2 (b) and *MVitDD* distribution for skin type 4 (c) in the central months of seasons.

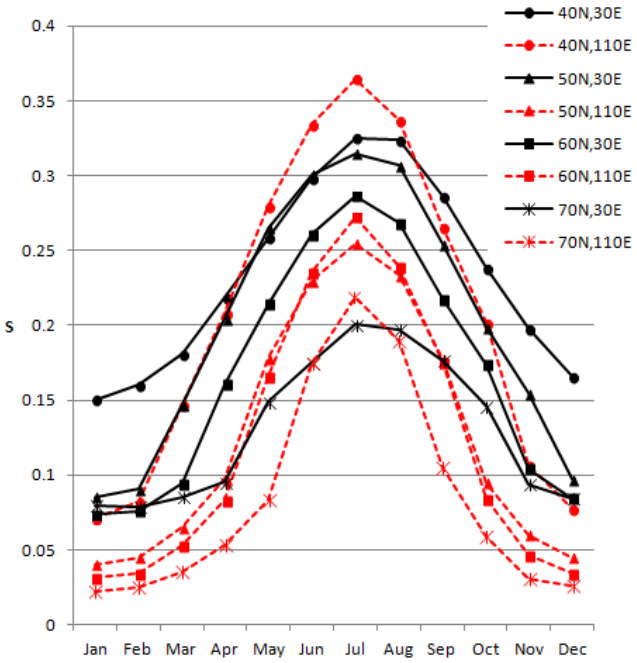

Fig. 3. Seasonal dependence of the open body fraction *S* at different latitudes and longitudes.

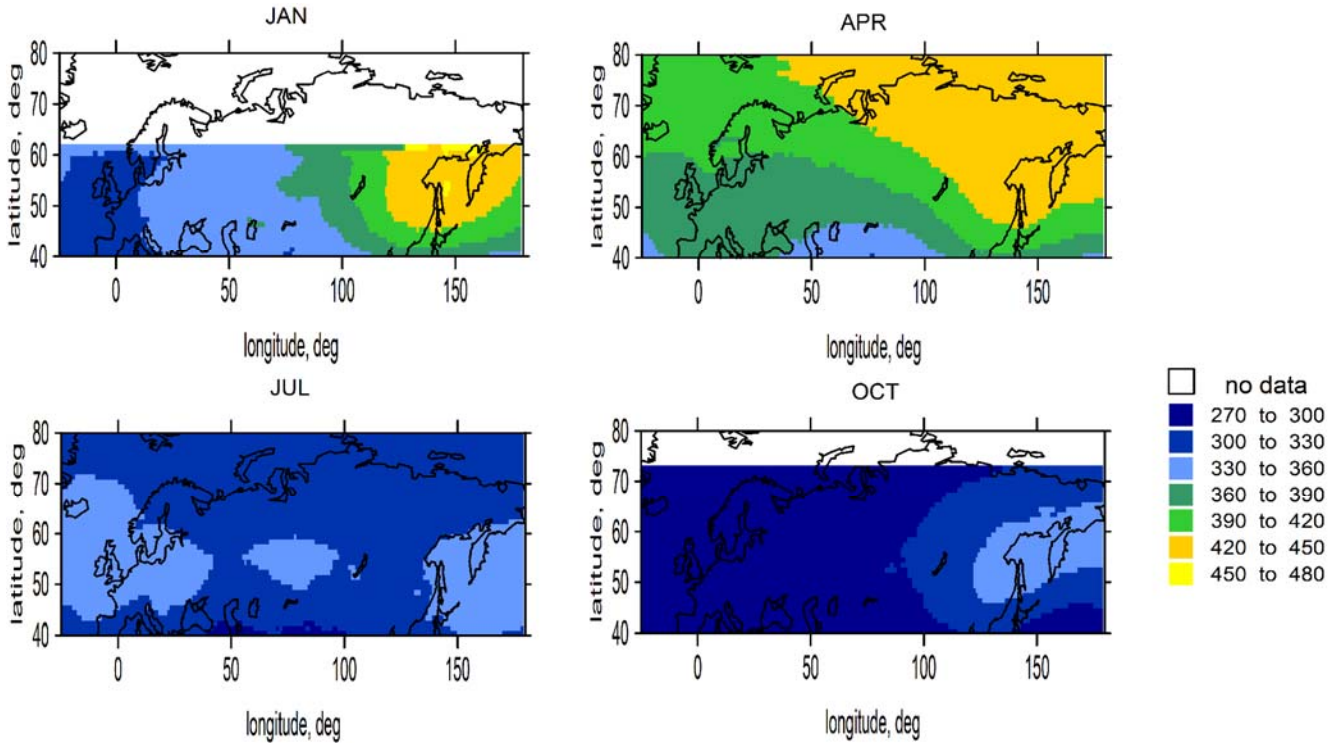

Fig. 4. The average total ozone distribution over Northern Eurasia according to the TOMS 1979-2003 data for different months.

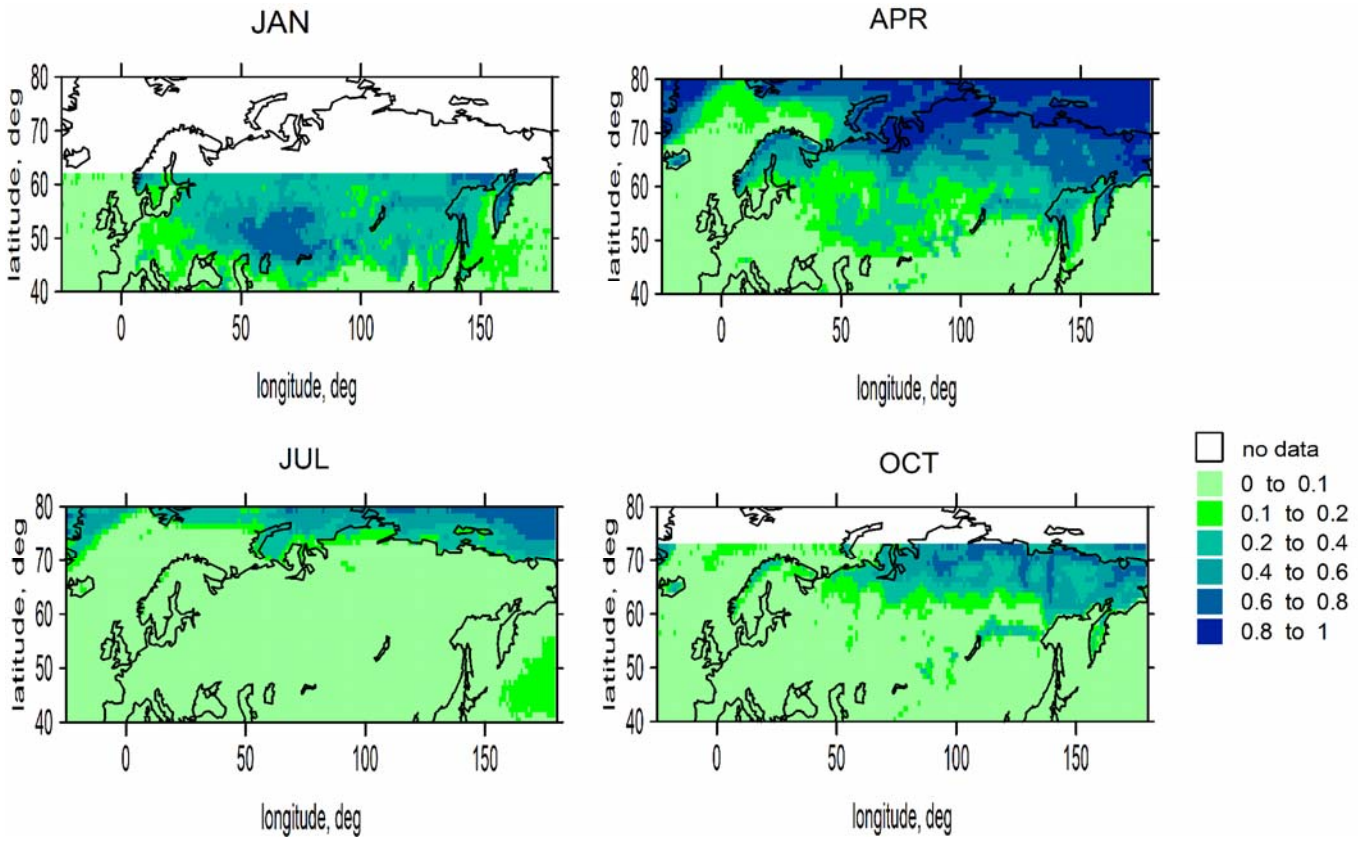

Fig. 5. The distribution of surface albedo according to the MTW technique [38,39]. See the details in the text.

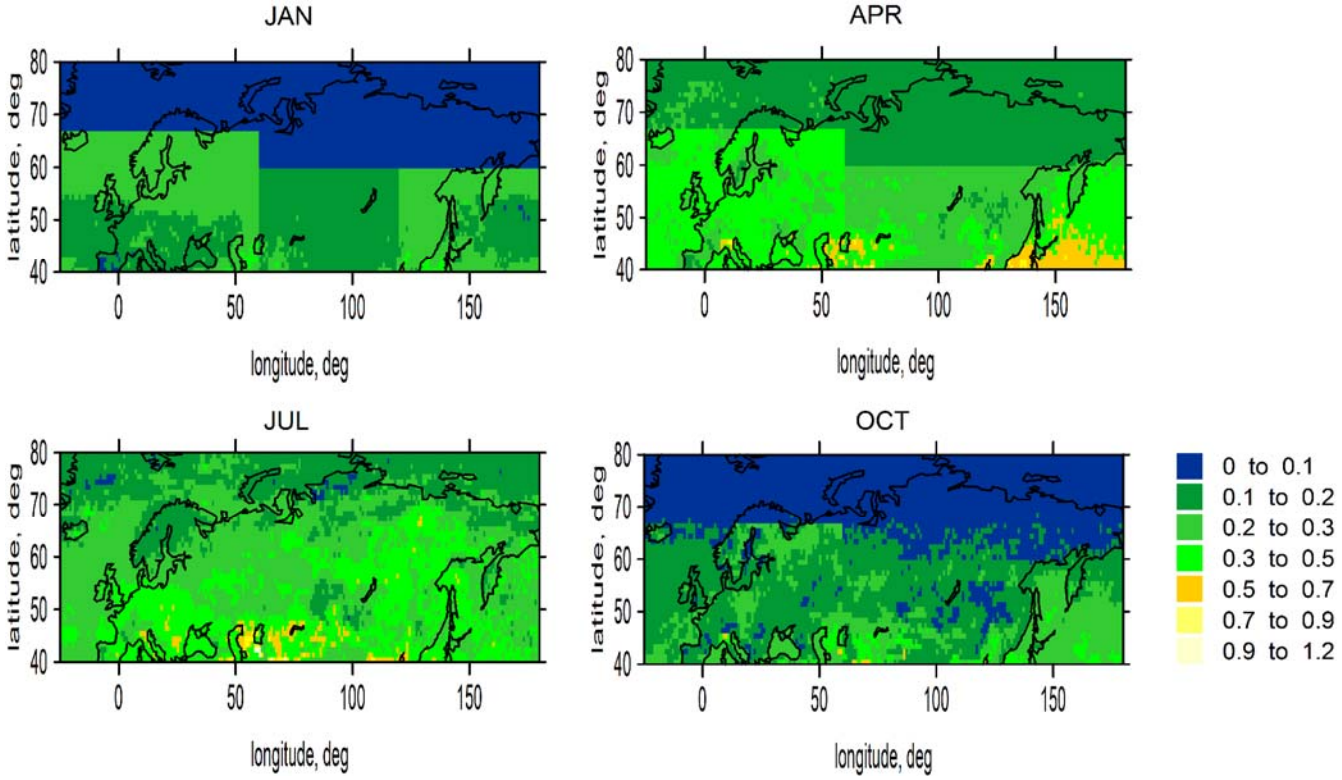

Fig. 6. Composite maps of aerosol optical thickness at 380 nm according to the MODIS, AERONET, and Russian actinometrical network data.

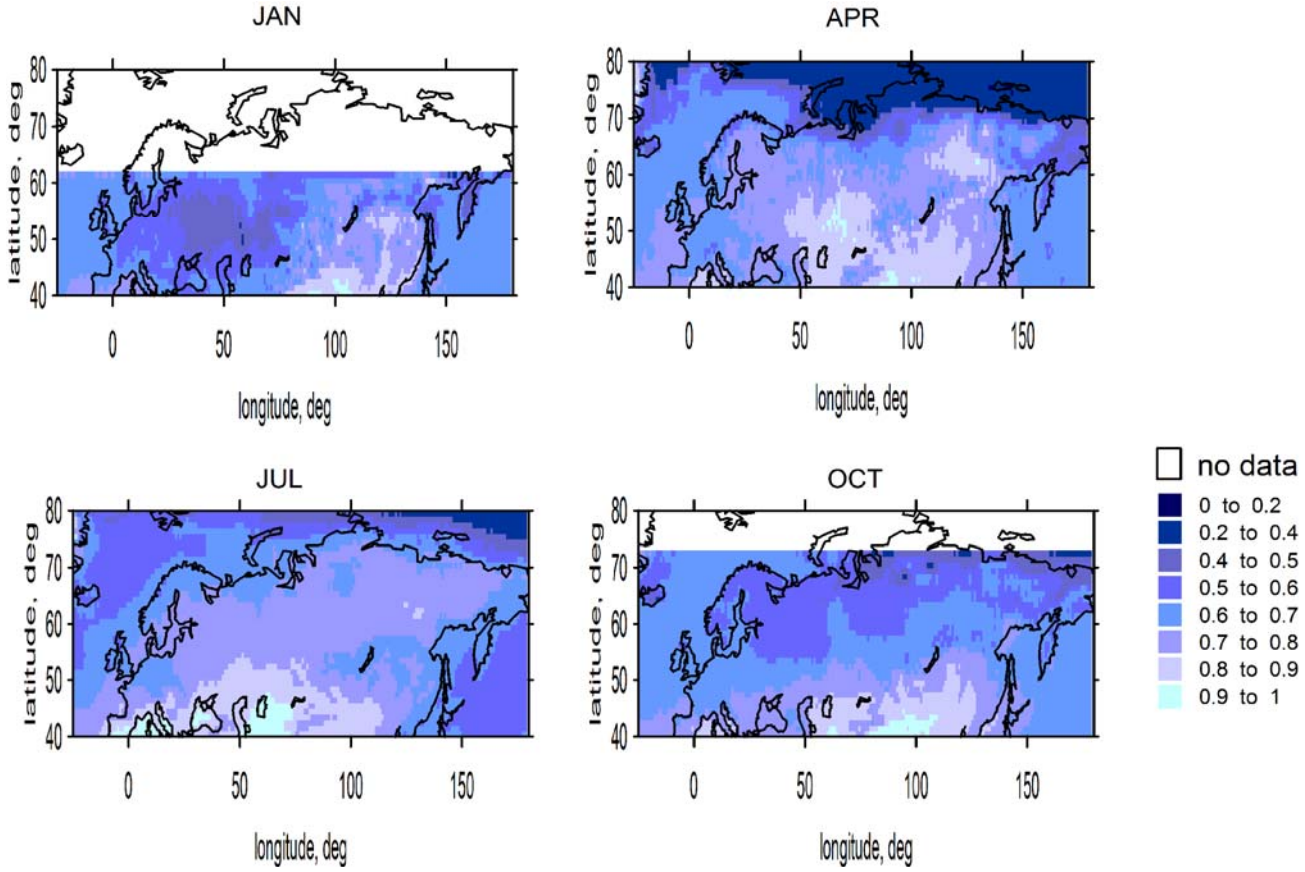

Fig. 7. The distribution of cloud modification factor *CMF* according to the developed method.

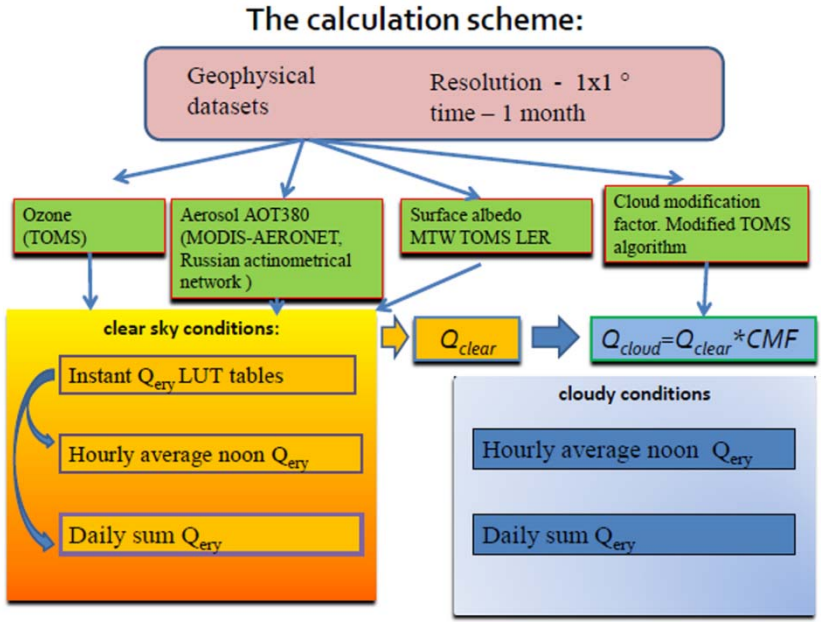

Fig. 8. The proposed scheme for calculation of UV resources.

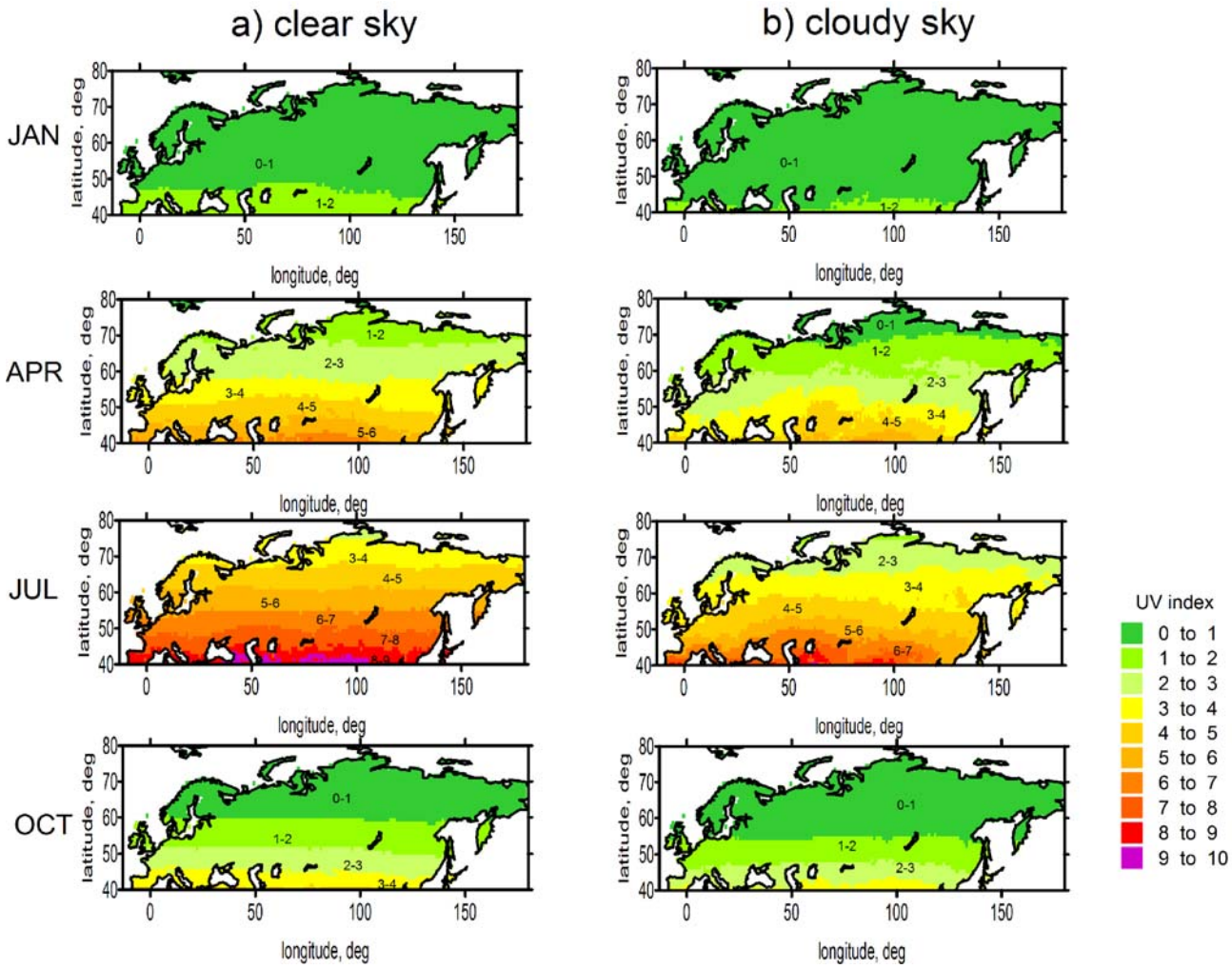

Fig. 9. UV index in clear sky and cloudy conditions at noon.

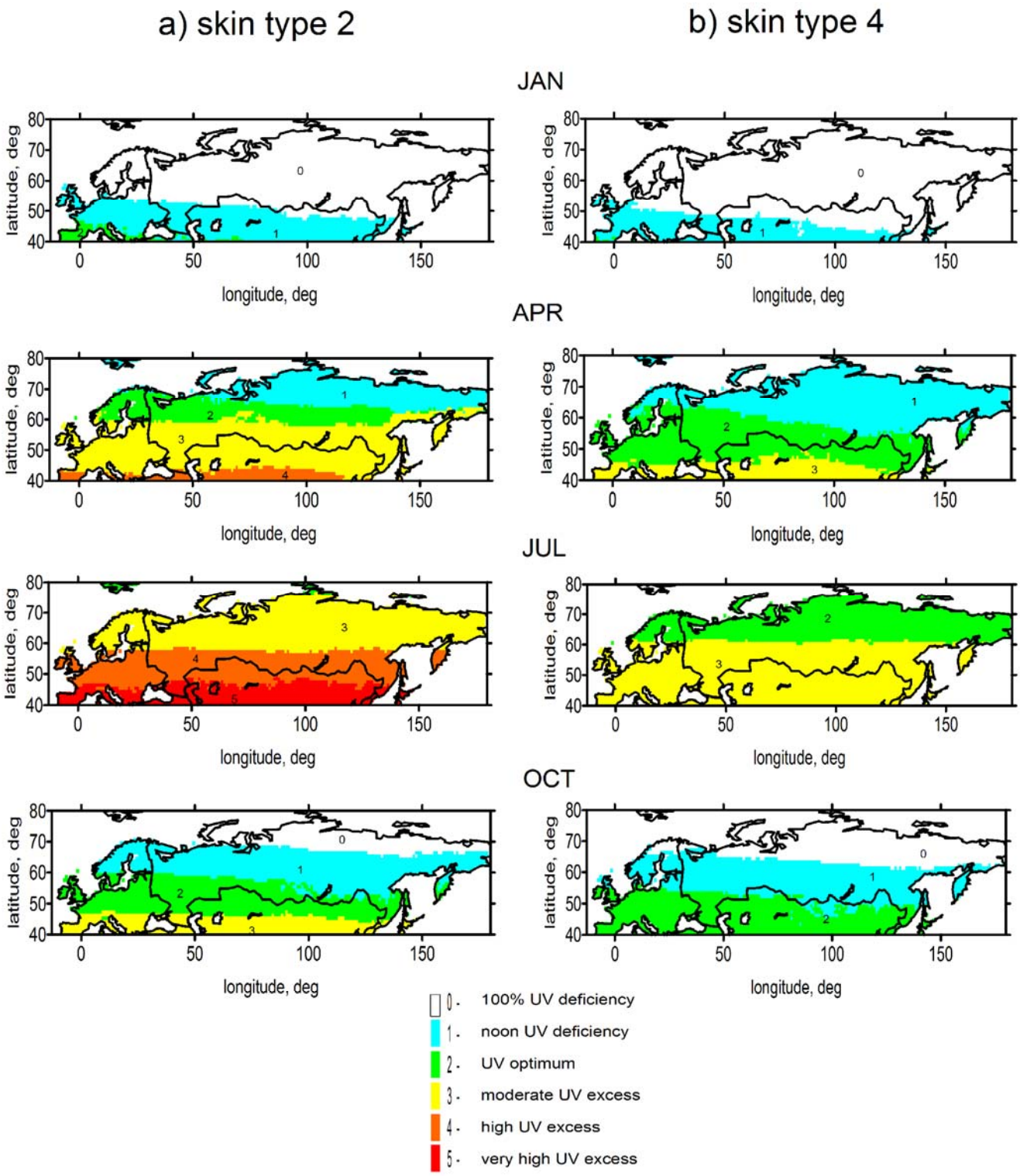

Fig. 10. The spatial distribution of UV resources for skin type 2 (a) and for skin type 4 (b). Clear sky conditions.

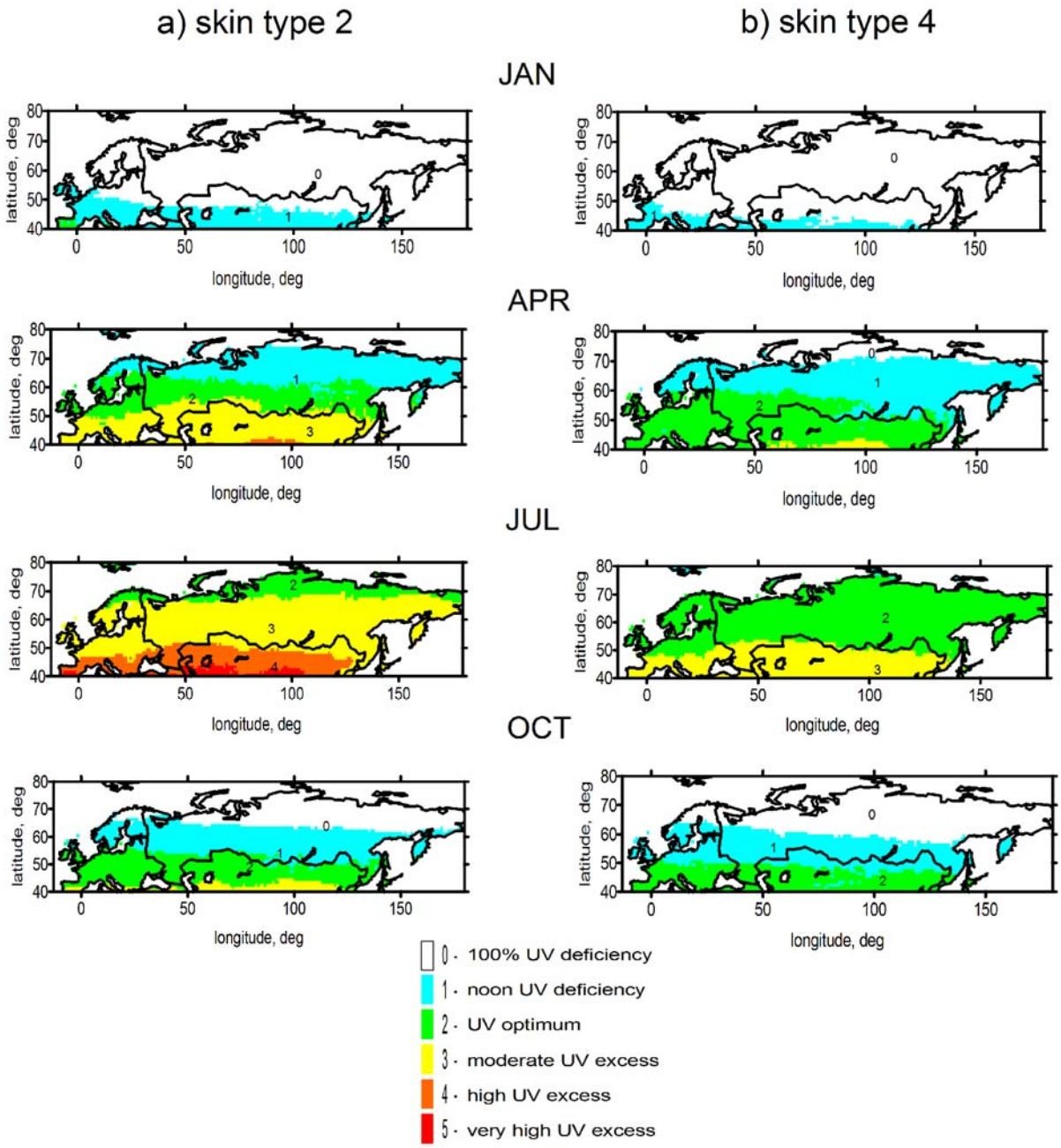

Fig. 11. The spatial distribution of UV resources for skin type 2 (a) and for skin type 4 (b). Mean cloudy conditions.

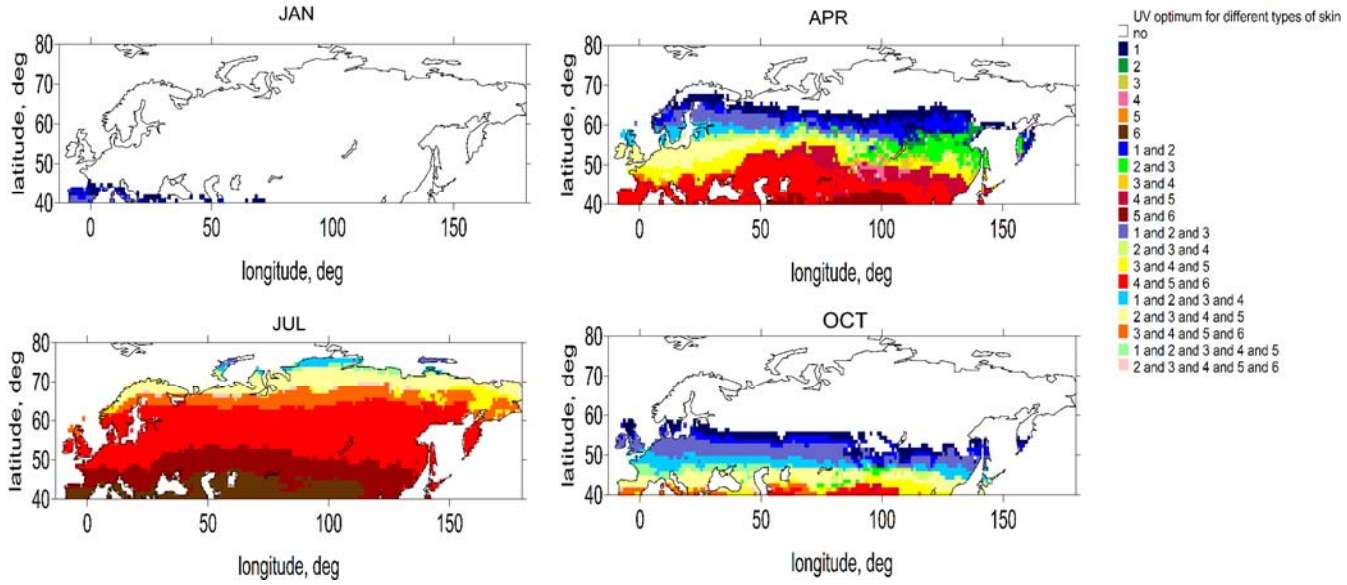

Fig. 12. The distribution of UV optimum for different skin types. Mean cloudy conditions.